Macromolecular
Theory and Simulation
www.mts-journal.d

Check for updates

Freely Suspended Semiflexible Chains in a Strong Aligning Field: Simple Closed-Form Solutions for the Small-Angle Approximation

Philipp A. Kloza and James A. Elliott*

A worm-like chain model for a single, freely suspended semiflexible macro-molecule with an aligning field of arbitrary coupling order is presented. Using a small-angle approximation and Ginzburg–Landau theory, exact closed-form solutions of the model are derived in the regime of a strong aligning field in arbitrary dimensions. Expressions for the mean cosine of the chain alignment angle, orientational order parameters, and the two-point correlation function are found. As a corollary, the persistence length is confirmed as a valid threshold for rigid behavior of the chain. The theoretical results are validated with Monte Carlo simulations in two and three dimensions. It is shown that the solutions for the small-angle approximation are within 0.1% of the simulated values for the exact model for chain-field alignment angles $\theta \lesssim 20°$. As a practical application, the findings are applied to carbon nanotubes in an aligning electric field.

1. Introduction

Describing the behavior of 1D polymer chains or semiflexible fibers in an external field is a problem that arises in many different areas of physics. In particular, the alignment of biological macromolecules such as DNA has been a major focus of past research due to its relevance in improving sequencing[1,2] and the emergence of single-molecule manipulation using atomic force microscopy and optical tweezers.[3] Similarly, electric fields have been used to align carbon nanotubes (CNTs) in an effort to improve their bulk electric and mechanical properties.[4,5]

Several theoretical treatments of the problem exist in the literature. The alignment of polarizable rigid rods suspended in air has been studied by analyzing the polarization of high aspect ratio ellipsoids subjected to Brownian bombardment.[6] In order to include bending effects, these 1D structures can also be modeled using semiflexible chains, where the chain has a finite bending stiffness. Studies using the continuous worm-like chain (WLC) model[7] have computed force–extension curves and end-to-end distributions.[8–11] More recently, an empirically corrected interpolation formula was found for the force–extension relationship that nearly matches the exact numerical result for the WLC.[12] For continuous chain contour functions, one may apply the path integral formalism known from quantum mechanics[13,14] which can then be solved using mean-field theory[15] or approximations in the limit of short or long chains.[16] Exact analytical expressions for the partition function and the end-to-end distribution of the WLC model with an external field have been found for two and three dimensions.[17] However, the solution is formulated in Fourier–Laplace space and is expressed in terms of complicated continued fractions. This solution was subsequently used to derive the end-to-end distribution of the free WLC model for a fixed chain end in Fourier space in arbitrary dimensions,[18] and was also extended by a torsional stiffness component to compute the ring-closure probability of DNA.[19] Likewise, the exact end-to-end distribution was numerically computed by treating the WLC as an equivalent quantum particle[20] or by considering random walks under constraints in Fourier–Laplace space.[21]

WLC models under spatial constraints have also been studied in the past. In these models, the constraints are rigid walls which the chain cannot penetrate. Early work by Odijk[22] established the existence of three regimes: the rigid rod regime for short chains, a flexible chain regime for long chains and a transition regime in between. The theory was later extended to lyotropic polymer liquid crystals.[23] Later, the partition function of the WLC with a harmonic confinement potential in the infinitely long chain limit and a lower bound on the confinement free energy in a circular tube have been found.[24] Confinement free energies for different confinement geometries have been studied for the WLC model, for example, in square and circular tubes.[25,26] An extensive review of WLC confinement theory is provided in ref. [27]. Confinement of a WLC by a harmonic potential for the displacement in two dimensions has further been studied by using Markov processes to compute the displacement distribution of the chain contour.[28]

Alternatively, the structure can be modeled using the discrete Kratky-Porod model[29] which can be readily simulated with Monte Carlo (MC) techniques.[30] These techniques have been used to compute force-extension curves[31] and average shapes[32] of semiflexible chains. Furthermore, MC simulation

P. A. Kloza, Prof. J. A. Elliott
Department of Materials Science & Metallurgy
University of Cambridge
27 Charles Babbage Road, Cambridge CB3 0FS, UK
E-mail: jae1001@cam.ac.uk

The ORCID identification number(s) for the author(s) of this article can be found under https://doi.org/10.1002/mats.202000049.

was used to study confinement and different types of interactions of semiflexible chains.[33]

In this work, we are interested in studying the behavior of a single freely suspended, semiflexible chain in a uniform aligning field. We consider the WLC model with coupling to an external field of arbitrary order. We start from Landau and Lifshitz's derivation of the persistence length,[34] which we extend by adding an aligning field and subsequently apply a small-angle approximation to the alignment of the chain contour relative to the aligning field. Hence, we are able to derive simple closed-form solutions for the cosine of the angle of the chain contour relative to the aligning field, an orientational order parameter as well as the two-point correlation function in arbitrary dimensions as a function of the contour length. In addition, we derive a lower bound on the external field strength necessary to align an entire chain with the field to a certain angle. We propose a way to compute force-extension curves by interpolating a well-known weak-field limit and our strong-field results. By comparing this interpolated force-extension curve to existing work in the literature, we find good agreement between our model and the exact solution of the WLC. We validate our other theoretical results with MC simulations of a Kratky–Porod model, which is equivalent to the WLC model considered here in the continuum limit. Finally, we derive expressions for the field susceptibility of a conductive and linearly dielectric chain in the presence of an aligning electric field and apply the results to describe the alignment of CNTs. Our methodology provides a general framework for computing highly accurate and compact expressions for a wide variety of averages in the WLC model, setting it apart from many of the previous studies on this topic.

2. The Model

We characterize the contour of the chain using the d-dimensional normalized tangent vector $\hat{\mathbf{t}}(s)$ as a function of the contour length s. The system is then described by the following free energy functional:

$$F[\hat{\mathbf{t}}(s)] = \int_0^L ds \frac{a}{2}\left(\frac{d\hat{\mathbf{t}}(s)}{ds}\right)^2 - \kappa\,|\,\hat{\mathbf{t}}(s)\cdot\mathbf{E}\,|^\nu \tag{1}$$

where L is the length of the chain, a is the bending stiffness, κ is the field susceptibility and $\mathbf{E}$ is the external aligning field. Additionally, ν denotes the coupling order of the alignment with respect to the external field. The first term in Equation (1) simply corresponds to the classical WLC free energy[7] for curvature of the chain. In the second field coupling term, we have assumed that the system obeys $\mathbf{Z}_2$ symmetry under the transformation $\hat{\mathbf{t}}(s) \rightarrow -\hat{\mathbf{t}}(s)$. This is the case for aligning flows, gravitational gradients, and electric fields that polarize the chain in the direction of the field. If the chain possesses, for example, a non-zero spin density, and we are considering the coupling with an external magnetic field, then $\mathbf{Z}_2$ symmetry is no longer present. However, the approximations considered in this work are equally valid in the limit of a strong aligning field irrespective of said symmetry. Without loss of generality, we define our coordinate system in d dimensions such that only the last component of the external field $E_d \equiv E$ is non-zero. We denote the

angle of the tangent vector relative to the external field as $\theta(s)$ and write in terms of the tangent vector $\hat{\mathbf{t}}(s) = (\theta_1(s),\ldots,\theta_d(s))^\top$:

$$\cos^2(\theta(s)) = 1 - \sum_{i=1}^{d-1}\theta_i^2(s) \tag{2}$$

If we now assume that $\theta(s)$ and all $\theta_i(s)$ are small, we can find the following identity by Taylor expanding the squared cosine to second order:

$$\theta^2(s) \approx \sum_{i=1}^{d-1}\theta_i^2(s) = \theta^2(s) \tag{3}$$

where we have introduced the vector $\boldsymbol{\theta}(s) = (\theta_1(s),\ldots,\theta_{d-1}(s))^\top$. Likewise, the curvature term can be approximated to second order in $\boldsymbol{\theta}$ and $d\boldsymbol{\theta}/ds$. The free energy given in Equation (1) can now be approximated by

$$F[\hat{\mathbf{t}}(s)] \approx F[\boldsymbol{\theta}(s)] = \int_0^L ds\,\frac{a}{2}\left(\frac{d\boldsymbol{\theta}(s)}{ds}\right)^2 - \kappa E^\nu\left(1 - \frac{\nu}{2}\theta^2(s)\right) \tag{4}$$

The theory is now geometrically linear, that is, components of different dimensions are additive in the energy. In addition, the approximation of the field interaction term is exact in the case of $\nu = 2$ as can be seen from Equation (2). We remark that the free energy above is no longer symmetric under the transformation $\hat{\mathbf{t}}(s) \rightarrow -\hat{\mathbf{t}}(s)$, thus the original $\mathbf{Z}_2$ symmetry is broken. However, a new $\mathbf{Z}_2$ symmetry arises due to invariance of the approximate free energy under the transformation $\boldsymbol{\theta}(s) \rightarrow -\boldsymbol{\theta}(s)$.

3. Solving the Model

3.1. The Canonical Partition Function

According to Ginzburg–Landau theory, the approximate free energy functional in Equation (4) is minimal in equilibrium with respect to $\boldsymbol{\theta}(s)$. In order to later find averages for field quantities as a function of s, we split the integral into three ranges:

$$F[\boldsymbol{\theta}(s)] = F_1[\boldsymbol{\theta}_1(s)] + F_2[\boldsymbol{\theta}_2(s)] + F_3[\boldsymbol{\theta}_3(s)] \tag{5}$$

where the $\boldsymbol{\theta}_i$ have support on the ranges $[0, s_a]$, $[s_a, s_b]$, and $[s_b, L]$ respectively. The contour lengths s_a and s_b are variable and obey $0 \leq s_a \leq L$ and $s_a \leq s_b \leq L$. Ultimately, this splitting is necessary to independently vary the field values at arbitrary points along the contour, not just at the ends. Otherwise, the field values along the contour are subject to energy minimization and will not yield correct results upon statistical averaging. The splitting allows us to compute the correct averages for functions of s_a and s_b such as the two-point correlation function. For functions with a single contour length argument like single-point field averages, a splitting into two ranges would be sufficient. The free energy for a $\boldsymbol{\theta}_i(s)$ in a range $[x_a, x_b]$ is given by

$$F_i[\boldsymbol{\theta}_i(s)] = \int_{x_a}^{x_b} ds\,\frac{a}{2}\left(\frac{d\boldsymbol{\theta}_i(s)}{ds}\right)^2 - \kappa E^\nu\left(1 - \frac{\nu}{2}\theta_i^2(s)\right) \tag{6}$$

**ADVANCED
SCIENCE NEWS**
www.advancedsciencenews.com

**Macromolecular
Theory and Simulations**
www.mts-journal.de

We compute the variational derivatives of the free energies to find the minima of the corresponding functionals by setting the derivatives to zero:

$$
\delta F_i\left[\theta_i(s)\right] = \int_{x_a}^{x_b} ds\, a\, \frac{d\theta_i(s)}{ds} \cdot \frac{d\delta\theta_i(s)}{ds} + \nu\kappa E^\nu \theta_i(s) \cdot \delta\theta_i(s)
$$
$$
= -\int_{x_a}^{x_b} ds\left(a\frac{d^2\theta_i(s)}{ds^2} - \nu\kappa E^\nu \theta_i(s)\right) \cdot \delta\theta_i(s) = 0, \qquad (7)
$$
$$
\forall x_a, x_b, \delta\theta_i(s)
$$

In going to the second line, the first integrand was integrated by parts where the boundary term vanishes due to Dirichlet boundary conditions. We then obtain the following boundary value problems for the individual θ_i:

$$
a\frac{d^2\theta_i(s)}{ds^2} - \nu\kappa E^\nu \theta_i(s) = 0, \quad \theta_i(x_a) = \mathbf{y}_a, \quad \theta_i(x_b) = \mathbf{y}_b \qquad (8)
$$

for some boundary values $\mathbf{y}_a$, $\mathbf{y}_b$. Each boundary value problem can be easily solved and yields the general solution

$$
\theta_i(s) = \frac{e^{-s/\Lambda}}{e^{2x_a/\Lambda} - e^{2x_b/\Lambda}}\left[e^{x_a/\Lambda}\left(e^{2s/\Lambda} - e^{2x_b/\Lambda}\right)\mathbf{y}_a \right.
$$
$$
\left. + e^{x_b/\Lambda}\left(e^{2x_a/\Lambda} - e^{2s/\Lambda}\right)\mathbf{y}_b \right] \qquad (9)
$$

where $\Lambda = \sqrt{a/(\nu\kappa E^\nu)}$ denotes a characteristic length scale of the system. The boundary values for each range are given by

$$
\theta_1(0) = \theta_0, \quad \theta_1(s_a) = \theta_2(s_a) = \theta_a,
$$
$$
\theta_2(s_b) = \theta_3(s_b) = \theta_b, \quad \theta_3(L) = \theta_L \qquad (10)
$$

By substituting the general solution into the free energy functional in Equation (6), solving the integral and summing over the three ranges, the free energy functional breaks down into a function of the boundary conditions:

$$
F(\theta_0, \theta_a, \theta_b, \theta_L) = F_0 + \frac{1}{\beta}\left(g_1\theta_0^2 + g_2\theta_a^2 + g_3\theta_b^2 + g_4\theta_L^2\right.
$$
$$
\left. - g_5\theta_0\cdot\theta_a - g_6\theta_a\cdot\theta_b - g_7\theta_b\cdot\theta_L\right) \qquad (11)
$$

Above, we have introduced the ground state energy $F_0 = -\nu\kappa E^\nu L$, a characteristic energy $\mathcal{E} = \sqrt{\nu\kappa E^\nu a}$ and a number of factors:

$$
g_1 = \frac{1}{2}\coth(s_a/\Lambda)\beta\mathcal{E},
$$
$$
g_2 = -\frac{1}{2}\beta\mathcal{E}\,\mathrm{csch}(s_a/\Lambda)\sinh(s_b/\Lambda)\,\mathrm{csch}((s_a - s_b)/\Lambda),
$$
$$
g_3 = -\frac{1}{2}\beta\mathcal{E}\sinh((L-s_a)/\Lambda)\,\mathrm{csch}((L-s_b)/\Lambda)\,\mathrm{csch}((s_a - s_b)/\Lambda), \qquad (12)
$$
$$
g_4 = \frac{1}{2}\beta\mathcal{E}\coth((L-s_b)/\Lambda), \quad g_5 = \beta\mathcal{E}\,\mathrm{csch}(s_a/\Lambda),
$$
$$
g_6 = -\frac{2\beta\mathcal{E}e^{(s_a+s_b)/\Lambda}}{e^{2s_a/\Lambda} - e^{2s_b/\Lambda}}, \quad g_7 = \frac{2\beta\mathcal{E}e^{(L+s_b)/\Lambda}}{e^{2L/\Lambda} - e^{2s_b/\Lambda}}
$$

The dependence of the field solution on s_a and s_b is from now on implicitly included in the factors g_i and expressions thereof and will only be explicitly expressed when useful. As the physics at hand will not be affected by our choice of the ground state energy, we can rescale by F_0. Using the identity for the multivariate Gaussian integral, we may now compute the canonical partition function of the system:

$$
Z = \iiiint d\theta_0 d\theta_a d\theta_b d\theta_L e^{-\beta F(\theta_0,\theta_a,\theta_b,\theta_L)} = \left(\frac{\pi^4}{g_1 g_4 g_8 g_{10}}\right)^{\frac{d-1}{2}} \qquad (13)
$$

The above individual integrals are understood to be over $\mathbb{R}^{d-1}$ respectively which approximates the exact partition function for a steep Gaussian integrand. We have further introduced additional shorthands:

$$
g_8 = g_2 - \frac{g_5^2}{4g_1}, \quad g_9 = g_3 - \frac{g_7^2}{4g_4}, \quad g_{10} = g_9 - \frac{g_6^2}{4g_8} \qquad (14)
$$

3.2. Field Averages

3.2.1. Two-Point Correlation Function

Before we begin computing averages of the tangent vector, let us first consider in more detail how a scalar product $\hat{\mathbf{t}}_a \cdot \hat{\mathbf{t}}_b$ may be expressed in terms of the corresponding angle vectors θ_a and θ_b. The correlation function for the WLC model without any external field is well known:[34]

$$
\langle \hat{\mathbf{t}}_a \cdot \hat{\mathbf{t}}_b \rangle_{E=0} = e^{-\frac{\langle(\theta_b - \theta_a)^2\rangle}{2}} \qquad (15)
$$

We will now show that this expression is also true when we include a harmonic external potential as in Equation (4). Consider a function $f((\theta_b - \theta_a)^2)$ with Taylor expansion:

$$
f((\theta_b - \theta_a)^2) = \sum_{i=0}^\infty c_i(\theta_b - \theta_a)^{2i} \qquad (16)
$$

In a Gaussian ensemble, we can easily compute the following average:

$$
\langle(\theta_b - \theta_a)^{2i}\rangle = \left(\frac{1}{g_{11}}\right)^i \frac{\Gamma\left(\frac{d-1}{2}+i\right)}{\Gamma\left(\frac{d-1}{2}\right)} = \frac{\Gamma\left(\frac{d-1}{2}+i\right)}{\Gamma\left(\frac{d-1}{2}\right)}\left(\frac{2}{d-1}\right)^i \langle(\theta_b - \theta_a)^2\rangle^i \qquad (17)
$$

where $i \in \mathbb{N}_0$ and with g_{11} defining another abbreviated quantity:

$$
g_{11} = g_9 - \frac{(g_6 - 2g_9)^2}{4(g_9 + g_8 - g_6)} \qquad (18)
$$

In particular, this means that the average of any power of $(\theta_b - \theta_b)^2$ is simply a power of the average $\langle(\theta_b - \theta_b)^2\rangle$, up to a factor. There are two things we can learn from this fact. First, we may write for the average of the function f:

**ADVANCED
SCIENCE NEWS**
www.advancedsciencenews.com

**Macromolecular
Theory and Simulations**
www.mts-journal.de

$$\left\langle f\left((\theta_b - \theta_a)^2\right)\right\rangle = \sum_{i=0}^{\infty} c_i \left\langle (\theta_b - \theta_a)^{2i}\right\rangle$$

$$= \sum_{i=0}^{\infty} c_i \frac{\Gamma\left(\frac{d-1}{2} + i\right)}{\Gamma\left(\frac{d-1}{2}\right)} \left(\frac{2}{d-1}\right)^i \left\langle (\theta_b - \theta_a)^2\right\rangle^i \tag{19}$$

$$= g\left(\left\langle (\theta_b - \theta_a)^2\right\rangle\right)$$

In going to the second line, we have applied Equation (17) and then used the resulting series to define an analytic function g under the assumption of series convergence. Second, analyticity of g implies continuity and for any such function where the c_i are independent of E, the zero-field limit is given by

$$\lim_{E \to 0} g\left(\left\langle (\theta_b - \theta_a)^2\right\rangle\right) = g\left(\lim_{E \to 0} \left\langle (\theta_b - \theta_a)^2\right\rangle\right) \tag{20}$$

The above findings can be directly applied to the correlation function of the WLC model since $\hat{\mathbf{t}}_a \cdot \hat{\mathbf{t}}_b$ is a function of geometry only. First, the validity of the expression given in Equation (15) can be extended to the case of $E \neq 0$. Second, we find by Taylor expanding the exponential and comparing coefficients with the general form given in Equation (19):

$$\langle \hat{\mathbf{t}}_a \cdot \hat{\mathbf{t}}_b \rangle = e^{-\frac{\langle (\theta_b - \theta_a)^2 \rangle}{2}} \Leftrightarrow \hat{\mathbf{t}}_a \cdot \hat{\mathbf{t}}_b = {}_0F_1\left(\frac{d-1}{2}; -\frac{d-1}{4}(\theta_b - \theta_a)^2\right) \tag{21}$$

where $_pF_q$ denotes the generalized hypergeometric function.[35] For $d = 2$, we simply recover $\hat{\mathbf{t}}_a \cdot \hat{\mathbf{t}}_b = \cos(\theta_b - \theta_a)$ as expected.

We have already computed the mean squared relative angle in Equation (17) for which we explicitly write:

$$\left\langle (\theta_b - \theta_a)^2\right\rangle = \frac{(d-1)}{4\beta\mathcal{E}}\left(\coth(L/\Lambda) - 1\right)e^{-2(s_a + s_b)/\Lambda}\left(e^{s_a/\Lambda} - e^{s_b/\Lambda}\right)$$
$$\times \left(-2e^{(2(L+s_a)+s_b)/\Lambda} + e^{(2L+s_a)/\Lambda} - e^{(2L+s_b)/\Lambda}\right. \tag{22}$$
$$\left. + 2e^{(s_a + 2s_b)/\Lambda} + e^{(3s_a + 2s_b)/\Lambda} - e^{(2s_a + 3s_b)/\Lambda}\right)$$

By construction of the free energy, the above expression is only valid if $s_b \geq s_a$; s_a and s_b need to be swapped otherwise. This expression also defines the correlation function for any two points at s_a, s_b via Equation (21). By construction, the zero-field limit then evaluates to

$$\lim_{E \to 0} \langle \hat{\mathbf{t}}_a \cdot \hat{\mathbf{t}}_b \rangle = e^{-\frac{|s_b - s_a|}{L_p}} \tag{23}$$

with L_p denoting the persistence length:[34]

$$L_p = \frac{2}{d-1}\beta a = \frac{2}{d-1}\beta\mathcal{E}\Lambda \tag{24}$$

With the expression for the correlation function found, one could in principle also compute the mean squared end-to-end distance of the chain using:

$$\langle R^2 \rangle = \int_0^L ds_a \int_0^L ds_b \langle \hat{\mathbf{t}}_a \cdot \hat{\mathbf{t}}_b \rangle \tag{25}$$

where s_a and s_b need to be swapped once $s_a > s_b$ as remarked before. In general, the integral has no closed-form solution due to the form of the correlation function. However, one may expand the exponential in the correlation function to find exact expressions for approximations to arbitrary order, or alternatively solve the above integral numerically.

3.2.2. Field Alignment

The right-hand side of Equation (21) also tells us how angles are generally measured in θ space. We may therefore compute the mean cosine of alignment (MCA) $\langle \cos\theta \rangle$ of the WLC with the external field direction $\hat{\mathbf{E}} = \mathbf{E}/E$ by choosing either $\hat{\mathbf{t}}_a$ or $\hat{\mathbf{t}}_b$:

$$\langle \cos\theta \rangle = \left\langle \hat{\mathbf{t}}_b \cdot \hat{\mathbf{E}}\right\rangle = \left(\frac{g_{10}}{\pi}\right)^{\frac{d-1}{2}} \int \theta_b \, {}_0F_1\left(\frac{d-1}{2}; -\frac{d-1}{4}\theta_b^2\right)e^{-g_{10}\theta_b^2}$$
$$= e^{-\frac{d-1}{4g_{10}}} = e^{-\frac{d-1}{2\beta\mathcal{E}}\operatorname{csch}(L/\Lambda)\cosh(s_b/\Lambda)\cosh((L-s_b)/\Lambda)} \tag{26}$$

Choosing $\hat{\mathbf{t}}_a$ instead will lead to the same result with s_b being replaced by s_a. Thus, we will drop the suffices a, b in the expression for the MCA henceforth. In the case of $d = 1$, both the correlation function and the MCA are unity as expected. Furthermore, the zero-field limit is not defined as there is no preferred direction. As Equation (26) is monotonically increasing on $[0, L/2]$ and is symmetric with respect to $L/2$, the minimum and maximum of the MCA are given by

$$\left\langle \hat{\mathbf{t}} \cdot \hat{\mathbf{E}}\right\rangle_{\min} = e^{-\frac{d-1}{2\beta\mathcal{E}}\coth(L/\Lambda)},$$
$$\left\langle \hat{\mathbf{t}} \cdot \hat{\mathbf{E}}\right\rangle_{\max} = e^{-\frac{d-1}{4\beta\mathcal{E}}\coth(L/(2\Lambda))} \tag{27}$$

Practically, one could be interested in determining the minimum field strength $E_{\min}$ necessary to align an entire chain to a certain value $\alpha \equiv \langle \hat{\mathbf{t}} \cdot \hat{\mathbf{E}} \rangle_{\min}$. Generally, the expression for the minimum MCA in Equation (27) is not analytically solvable for E. However, we may study the limits of short and long chains. For small L, $\coth(L/\Lambda) \approx \Lambda/L$ and for large L, $\coth(L/\Lambda) \approx 1$. Hence, we may solve for $E_{\min}$ in both limits:

$$E_{\min} \approx \begin{cases} \left(\dfrac{1-d}{2\beta\nu\kappa L \ln\alpha}\right)^{\frac{1}{\nu}}, & \text{for } L \ll L^*, \\[3mm] \left(\dfrac{1-d}{2\beta\sqrt{\nu\kappa a}\ln\alpha}\right)^{\frac{2}{\nu}}, & \text{for } L \gg L^* \end{cases} \tag{28}$$

Above, L^* denotes the threshold where both approximations are equal. It can be expressed in terms of the persistence length as

$$L^* = -\ln\alpha L_p \tag{29}$$

It turns out that short chains with $L \ll L^*$ can be treated as rigid rods for any given α as the approximate expression in Equation (28) does not depend on the bending stiffness a anymore. Indeed, it is simple to verify that the short chain limit is identical to taking the limit $a \to \infty$, corresponding to an infinitely stiff and thus rigid chain or rod. Additionally, the minimum and maximum MCA along the chain coincide in this limit since the alignment is no longer a function of contour length, further supporting the rigid rod interpretation. According to Equation (24), the persistence length increases with stiffness and decreases with temperature. Therefore, the rigid rod approximation holds for stiff and short chains at low temperatures. For $L \gg L^*$ on the other hand, finite length effects are negligible, but bending of the chain becomes relevant. This leads to the existence of a lower bound for the required electric field strength given by the large L limit in Equation (28).

3.2.3. Orientational Order Parameter

A quantity that is useful for quantifying the alignment irrespective of the relative sign of the tangent vector and the reference axis is the squared cosine of the alignment angle:

$$
\begin{aligned}
\langle \cos^2 \theta \rangle &= \left\langle \left(\hat{\mathbf{t}} \cdot \hat{\mathbf{E}} \right)^2 \right\rangle = \left(\frac{g_{10}}{\pi} \right)^{\frac{d-1}{2}} \int d\theta_b \, _0F_1^2 \left(\frac{d-1}{2} ; -\frac{d-1}{4} \theta_b^2 \right) e^{-g_{10}\theta_b^2} \\
&= {}_1F_1 \left(\frac{d-2}{2} ; d-2 ; -\frac{d-1}{g_{10}} \right) \\
&= {}_1F_1 \left(\frac{d-2}{2} ; d-2 ; -\frac{2(d-1)}{\beta \mathcal{E}} \right. \\
&\quad \left. \operatorname{csch}(L/\Lambda) \cosh(s_b/\Lambda) \cosh((L-s_b)/\Lambda) \right)
\end{aligned}
\tag{30}
$$

The average also appears in the expansion of the orientation distribution function (ODF) of a system in terms of spherical harmonics.[36] If the ODF is symmetric about an axis, then the expansion is in terms of Gegenbauer polynomials.[35] The second moment of the expansion is commonly used as an orientational order parameter of polymeric and macromolecular systems which we will denote as σ. In two[37] and three[38] dimensions it is given by

$$
\sigma_{2D} = \langle T_2(\cos \theta) \rangle = 2\langle \cos^2 \theta \rangle - 1
\tag{31}
$$

$$
\sigma_{3D} = \langle P_2(\cos \theta) \rangle = \frac{1}{2} \left(3\langle \cos^2 \theta \rangle - 1 \right)
\tag{32}
$$

for a choice of $\hat{\mathbf{E}}$ as the reference axis. Above, T_2 and P_2 denote the Chebyshev and Legendre polynomials as special cases of the Gegenbauer polynomials in two and three dimensions.[35] In two dimensions, the order parameter $\sigma_{2D} = 1$ for perfect field alignment and $\sigma_{2D} = -1$ for a fully orthogonal orientation with respect to the field. In three dimensions, these two extremes correspond to order parameters of $\sigma_{3D} = 1$ and $\sigma_{3D} = -1/2$ respectively.

3.2.4. Chain Extension

Similar to the squared end-to-end distance, the mean chain extension in the direction of the field can be computed numerically by evaluating the following integral of the MCA:

$$
\langle R_d \rangle_{SF} = \int_0^L ds \, \langle \cos \theta(s) \rangle
\tag{33}
$$

Due to our assumptions of small angles and a strong aligning field, the above integral will only yield good results where these assumptions hold, which we indicate by the suffix SF. In order to improve the accuracy of the extension-field relationship, one common approach is to interpolate between the weak- and strong-field limits.[8] In the literature, the most commonly discussed aligning field is of order $\nu = 1$,[8,12,17] which we will assume for the remainder of this section. Such a field is then typically referred to as a "force" in the literature. In the weak-field limit, the extension of the chain simply follows from the equipartition theorem and is given by a linear relationship:[8]

$$
\langle R_d \rangle_{WF} = \frac{4\kappa E a \beta^2 L}{d(d-1)}
\tag{34}
$$

The interpolation is typically performed in the aligning field, that is, the field is treated mathematically as the response to an extension.[8] For strong fields, the asymptotic field response is known and diverges as:[8]

$$
E = \frac{(d-1)^2}{16\kappa a \beta^2 (1 - \langle R_d \rangle / L)^2}
\tag{35}
$$

If we were to just add the field responses, the linear contribution from the weak-field response would be added on top of a linear term arising from Taylor expanding Equation (35) in $\langle R_d \rangle$:

$$
E_{lin}(\langle R_d \rangle) = \frac{(d-1)^2 \langle R_d \rangle}{8\kappa a \beta^2 L}
\tag{36}
$$

To correct these double contributions and ensure the correct behavior for weak fields, the above linear term needs to be subtracted from the strong-field response. Furthermore, the strong-field response given in Equation (33) is not analytic for $E = 0$ due to the functional form of the MCA. Therefore, a smooth cutoff factor needs to be applied to the strong-field response for small extensions. Otherwise, the interpolation will not give the correct weak-field limit. All these aspects are considered in the following expression for the "interpolated" field:

$$
E_I(\langle R_d \rangle) = E_{WF}(\langle R_d \rangle) + \left(1 - e^{-\langle R_d \rangle / L_p} \right) \left[E_{SF}(\langle R_d \rangle) - E_{lin}(\langle R_d \rangle) \right]
\tag{37}
$$

where $E_{SF}(\langle R_d \rangle)$ and $E_{WF}(\langle R_d \rangle)$ are the inverses with respect to E of Equations (33) and (34) respectively. In the exponential term, we chose the persistence length as the decay length; however, any choice that is much smaller than the chain length will produce results similar to the ones discussed later in this section. Finally, the function in Equation (37) can be inverted again to yield the interpolated extension $\langle R_d \rangle_I$ as a function of E. In $d = 3$ dimensions and for non-dimensional values $\beta = a = \kappa = 1$, we
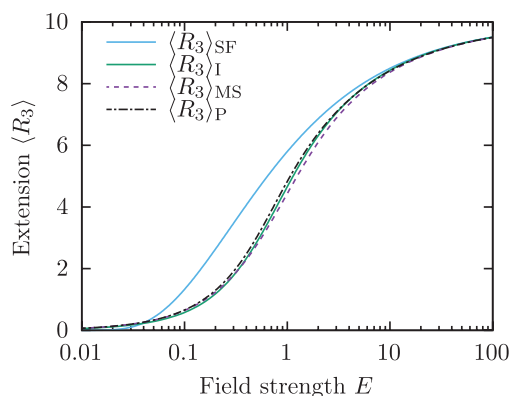
Figure 1. Lin-log plot of extension vs field strength. Comparison of results from this work obtained through the small-angle approximation (SF) and interpolation (I) with literature results by Marko and Siggia (MS)[8] and Petrosyan (P).[12]

compare our results for the extension with results from the literature in **Figure 1**. We chose two studies that consider a WLC model that is equivalent to ours with $v = 1$ and without the modulus in Equation (1). As noted before, the modulus does not matter in the strong-field regime. The first study by Marko and Siggia (suffix MS)[8] provides a well-known result for the force-extension curve which was derived by interpolating weak- and strong-field results. The interpolation approach described above is also formally equivalent to the one used by Marko and Siggia. The second study is by Petrosyan (suffix P) which empirically corrects the Marko–Siggia result and is within 1% of the exact solution.[12] Hence, the result by Petrosyan can be effectively used to compare our results to the exact solution. Furthermore, $L = 10.0$ was chosen as both studies only produce correct results if $L \gg L_p$.[8] All results visually coincide for field strengths $E > 10.0$. As expected, the small-angle approximation overestimates the alignment and hence the extension of the chain as the harmonic potential is steeper than the corresponding exact cosine term. However, our approach has several advantages over the cited studies. First, it is valid for all values of L and not limited to long chains. Furthermore, our interpolated result is closer to the exact result of the WLC than the Marko-Siggia result starting at relatively low field strengths of $E > 0.5$ while only very slightly underestimating the extension

for weaker fields. This difference can be explained by the fact that Marko and Siggia merely use the asymptotic behavior of the strong-field solution given by Equation (35) whereas we use the exact solution of the small-angle approximation for all possible field strengths. Our approach also does not rely on empirically corrected interpolation formulae compared to the result derived by Petrosyan.[12] Finally, the methodology described in this work allows for the computation of a wide variety of relevant averages, not only the chain extension.

4. Validation with Monte Carlo Simulation

By discretizing the free energy expression, we may cast the model into a form which can be easily simulated using an MC approach. The discretized version is also known as the Kratky-Porod model.[29] The chain is discretized into N straight segments with length l and normalized vector $\hat{\mathbf{t}}_i$ for which we can write down the following energy expression:

$$F(\{\hat{\mathbf{t}}_i\}) = \sum_{i=1}^{N-1} \frac{a}{2l} \hat{\mathbf{t}}_i \cdot \hat{\mathbf{t}}_{i+1} - \sum_{i=1}^{N} \kappa l \, |\hat{\mathbf{t}}_i \cdot \mathbf{E}|^v \tag{38}$$

In the small-angle approximation, the expression simplifies to:

$$\overline{F}(\{\theta_i\}) = \sum_{i=1}^{N-1} \frac{a}{2l} (\theta_{i+1} - \theta_i)^2 - \sum_{i=1}^{N} v \kappa l \, \theta_i^2 \tag{39}$$

where the θ_i are $d - 1$ dimensional vectors analogous to the continuous field and we have shifted the energy by F_0 as before. Both the exact and approximate Kratky-Porod model can be easily simulated using an MC algorithm with Rosenbluth sampling[39] to accelerate the computational convergence. For the theoretically derived expressions in Equations (21) and (26), one can confirm the validity of the results with an MC simulation of a system with the free energy given by Equation (39). For our purposes, we set $\beta = a = \kappa = v = L = E = 1$ and use $N = 500$ discrete segments. The simulation results are in excellent agreement with the analytical expressions, as shown in **Figure 2**.

Furthermore, we can also simulate the system for the exact potential given in Equation (38) and compare it to the theoretical predictions derived for the approximate potential. Here, we
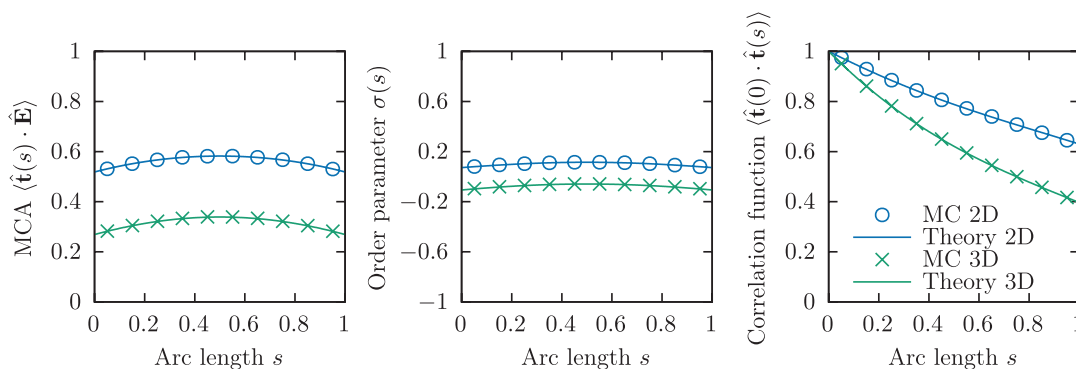

Figure 2. Comparison of theoretical prediction and MC simulation results with the approximate potential for MCA, order parameter and correlation function function vs. contour length.

**ADVANCED
SCIENCE NEWS**

www.advancedsciencenews.com

**Macromolecular
Theory and Simulations**
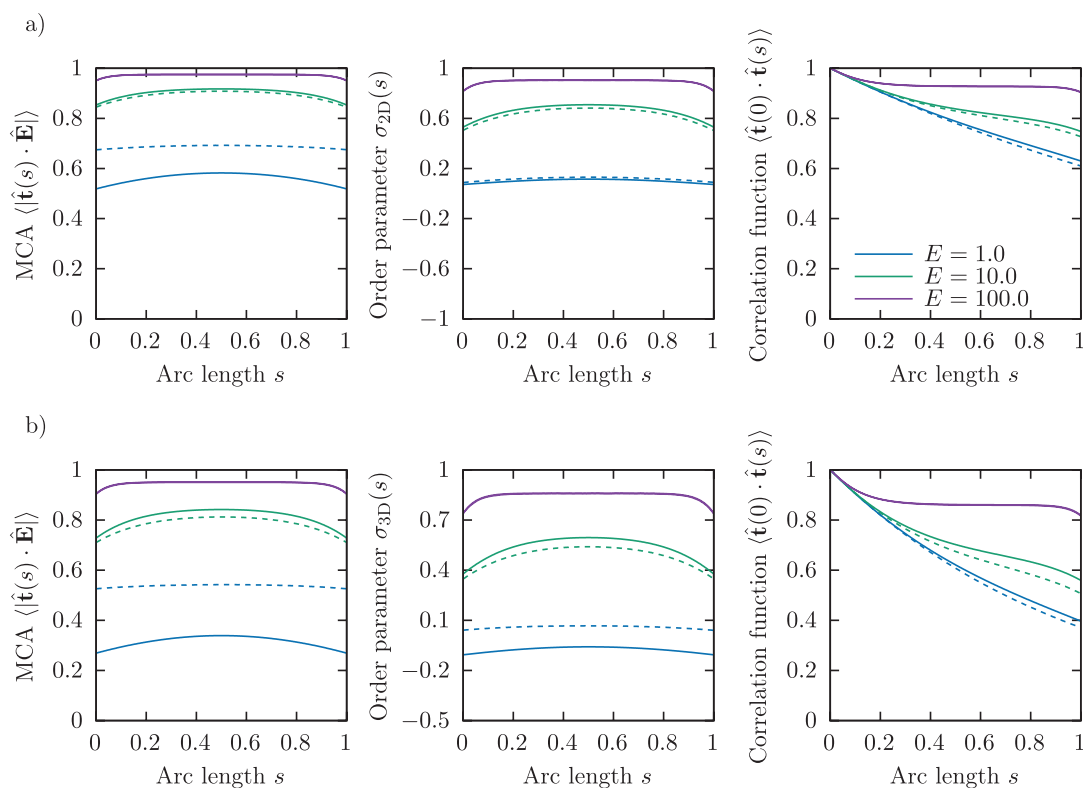
www.mts-journal.de

Figure 3. Comparison of MC simulation results and theoretical predictions for MCA, order parameter and correlation function for $d = 2$ (a) and $d = 3$ (b). Solid lines are values predicted by theory and dashed lines are values obtained from MC simulations.

note that the MCA for the exact potential in the MC simulations is measured as $\langle |\hat{\mathbf{t}}(s) \cdot \hat{\mathbf{E}}| \rangle$ due to the underlying $\mathbf{Z}_2$ symmetry while the approximate theory provides values for $\langle \hat{\mathbf{t}}(s) \cdot \hat{\mathbf{E}} \rangle$. Otherwise, we would be measuring a vanishing average due to the spontaneous symmetry breaking into broadly aligned or anti-aligned orientations with respect to the external field. For weak fields, the modulus should lead to a higher degree of alignment being measured with the exact potential compared to the case where no $\mathbf{Z}_2$ symmetry is considered as all contributions to the average are positive. In addition, the existence of two minima as attractors in orientation space leads to a larger number of aligned configurations for the exact potential as long as the energy barrier between both minima is sufficiently low so that a single configuration may span both. Hence, we should observe higher values for the MCA and orientational order parameter with the exact potential compared to the approximate potential. For strong fields, the two potential wells of the exact potential for opposite chain orientations with respect to the external field become increasingly disjoint in probability space, such that $\mathbf{Z}_2$ is effectively broken for each generated configuration. Both resulting sets of configurations are equivalent to each other, equally probable and can be both approximated by the small-angle approximation with broken symmetry. Then, the approximate harmonic potential presents a steeper potential well than the exact expression, resulting in a higher MCA as well as a higher orientational order parameter.

These predictions are confirmed by the converged MC results shown in **Figure 3** where they are compared to theoretical predictions in two and three dimensions. For the simulations, we

used the same values as listed above and merely varied the external field strength E. While the results deviate significantly for a weak aligning field ($E = 1.0$) for the MCA of the chain with the field, the agreement between theory and simulation improves with increasing field strength and both results visibly coincide at $E = 100.0$ in both two and three dimensions. This can be explained by the decrease of the alignment angle with respect to the field with increasing field strength where the small-angle approximation becomes more valid until the results are visibly indistinguishable. Additionally, one observes that the MCA and order parameter for the exact potential are higher in the case of $E = 1.0$ compared to the approximate potential and lower for greater field strengths. These findings are therefore in full agreement with our previous discussion.

As the correlation function measures relative angles and the order parameter is an even function of the alignment angle, they are not subject to any adjustment in the measurement unlike the MCA. We therefore observe significantly better agreement with theory in the weak field regime. The order parameter behaves qualitatively like the MCA but with a better quantitative agreement with theory. For the correlation function, simulations and theory diverge slightly in the medium field regime where the small-angle approximation is not fully valid yet and subsequently converge for strong fields. This leads to the conclusion that any approximation to the squared end-to-end distance based on the theoretically derived correlation function will agree well with its corresponding exact value.

One also observes generally greater alignment with the field close the center of the chain compared to the chain ends due
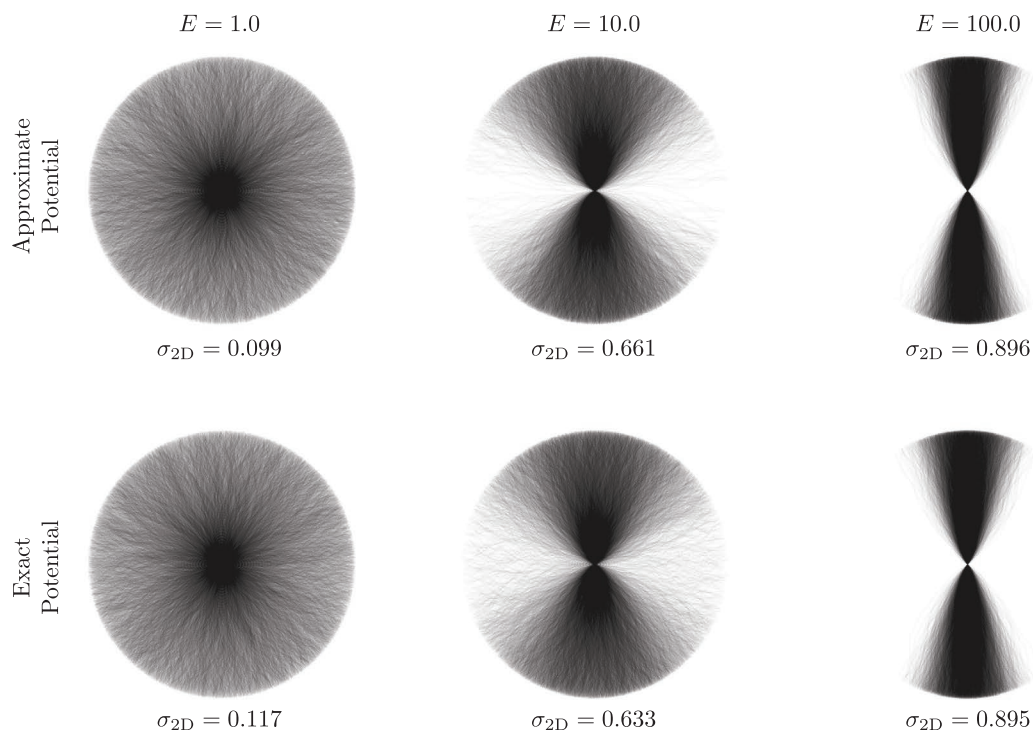
Figure 4. Visualization of 10 000 ensemble configurations for different field strengths in the approximate and exact potentials in two dimensions. Aligning field pointing upwards with all chain configurations overlaid at the chain midpoint. Images are annotated with corresponding order parameters converged to the shown decimal places.

to the stronger coupling of the elastic and aligning fields. In $d = 3$ dimensions, our theoretical predictions agree well with the simulation results for $\langle \hat{\mathbf{t}} \cdot \hat{\mathbf{E}} \rangle > 0.75$ or an alignment angle $\theta \lesssim 40°$ with a maximum error in the MCA of less than 5%. The agreement becomes excellent with a maximum MCA error of less than 0.1% in the regime $\langle \hat{\mathbf{t}} \cdot \hat{\mathbf{E}} \rangle > 0.95$ or $\theta \lesssim 20°$.

The MC simulation results can also be directly visualized by overlaying a large number of generated configurations as is shown in **Figure 4** for two dimensions. By choosing to overlay all configurations at the midpoint of the chain, it is possible to compare configurations generated from theories with and without $\mathbf{Z}_2$ symmetry in the tangent vectors $\hat{\mathbf{t}}_i$. At first glance, the results for the approximate and exact potentials look very similar, though one may observe minor differences consistent with the observations discussed before. For $E = 1.0$, the dark central region is vertically elongated for the exact potential compared to the approximate potential, suggesting greater field alignment as noted before. This greater field alignment is also supported by a greater order parameter being measured for the exact potential. The order parameter was averaged over all chain segments. In the case of the two higher field strengths, the opposite can be observed: the top and bottom lobes for the exact potential "fan out" more widely than for the approximate potential, though the difference is barely noticeable at $E = 100.0$. Likewise, the order parameters are greater for the approximate potential in those cases, with the values only differing in the third decimal place at the highest applied field strength.

5. Application to Alignment of Carbon Nanotubes in an Electric Field

5.1. Properties of Carbon Nanotubes

Since their first correct identification,[40] CNTs have been a subject of major scientific and technological interest due to their exceptional mechanical, electrical and thermal properties. A practical application of our theory is the alignment of CNTs by electromagnetic fields with the goal of producing materials with high mechanical stiffness and strength as well as high electrical conductivity in the alignment direction.[41] In particular, CNTs produced using the floating catalyst chemical vapor deposition (FCCVD) method[42] are suitable for alignment by an electric field as they are freely suspended in hydrogen gas during synthesis. We will focus on the alignment of CNTs during synthesis in the FCCVD furnace, in contrast to post-synthesis alignment, for example, during the embedding of the CNTs in an epoxy matrix.[43] We present a preliminary demonstration of how the theory can be applied in practice and a more definitive analysis of the problem of CNT alignment will be described in future work.

Here, we provide a brief summary of the structural and electrical properties of CNTs following ref. [44]. The structure of a single-wall CNT (SWCNT) is fully characterized by the chiral vector $\mathbf{C}_h = (n, m)$ with chiral indices $n, m \in \mathbb{N}_0$. SWCNTs where the chiral indices satisfy $n - m = 3k$ with $k \in \mathbb{Z}$ are metallic; they do not have a band gap and are thus conductive. In contrast,

**ADVANCED
SCIENCE NEWS**
www.advancedsciencenews.com

**Macromolecular
Theory and Simulations**
www.mts-journal.de

all other SWCNTs do have a band gap and are semiconductors, hence show dielectric behavior. The FCCVD method typically produces both metallic and semiconductive SWCNTs,[45] hence the two cases will be analyzed in turn.

5.2. Conductive Chain

Let $\mathbf{E}$ be an external electric field. We will assume that charges in the chain can only move parallel to the chain contour. Thus, we may split the electric field into two components, one parallel to the contour and one perpendicular to it:

$$\mathbf{E}(s) = \mathbf{E}_\perp(s) + \mathbf{E}_\|(s); \quad \mathbf{E}_\perp(s) \cdot \hat{\mathbf{t}}(s) = 0, \quad \mathbf{E}_\|(s) \cdot \hat{\mathbf{t}}(s) = \| \mathbf{E}_\|(s) \| \qquad (40)$$

The parallel component of the electric field is reduced to zero in a conductive chain due to moving charges. We use the difference in electric field energy as the coupling component to the external field. Additionally, the electric field is assumed to vanish within a constant cross-section A around the contour of the chain. Hence, we write for an electrically conductive WLC occupying a volume $\mathcal{V}_{\mathrm{WLC}}$:

$$F_{\mathrm{C}} = -\frac{\varepsilon_0}{2} \int\limits_{\mathcal{V}_{\mathrm{WLC}}} \mathrm{d}V \, \mathbf{E}_\|^2 = -\frac{\varepsilon_0}{2} A \int_0^L \mathrm{d}s \, | \mathbf{E} \cdot \hat{\mathbf{t}}(s) |^2 \qquad (41)$$

Thus, we may identify $\nu_{\mathrm{C}} = 2$ and $\kappa_{\mathrm{C}} = \varepsilon_0 A / 2$ for a conductive WLC in correspondence with our model.

5.3. Dielectric Chain

As with a conductive chain discussed above, we will assume that polarization in the dielectric case is only possible parallel to the chain contour, where it will be convenient to adopt the representation of the electric field vector given in Equation (40). In a linear dielectric with electric susceptibility χ, the component of the electric field parallel to the chain contour reduces according to:

$$\mathbf{E}'_\| = \frac{\mathbf{E}_\|}{1 + \chi} \qquad (42)$$

We deduce for the interaction energy of the dielectric with the aligning field:

$$F_{\mathrm{D}} = \frac{\varepsilon_0}{2} \int\limits_{\mathcal{V}_{\mathrm{WLC}}} \mathrm{d}V \, \mathbf{E}'^2_\| - \mathbf{E}^2_\| = -\frac{\varepsilon_0}{2} \frac{\chi^2 + 2\chi}{(1 + \chi)^2} A \int_0^L \mathrm{d}s \, | \mathbf{E} \cdot \hat{\mathbf{t}}(s) |^2 \qquad (43)$$

Again, we have assumed that the field is effectively reduced inside a cross-section A around the chain contour. As before, we have $\nu_{\mathrm{D}} = 2$ and the field susceptibility:

$$\kappa_{\mathrm{D}} = \frac{\varepsilon_0}{2} \frac{\chi^2 + 2\chi}{(1 + \chi)^2} A \qquad (44)$$

In the limit $\chi \to \infty$, we recover the field susceptibility of a conductor $\kappa_{\mathrm{D}} \to \kappa_{\mathrm{C}}$. Notice that $(\chi^2 + 2\chi)/(1 + \chi)^2 < 1$, hence a

conductive chain will always tend to align more with the field than its dielectric counterpart.

5.4. Field Alignment of Carbon Nanotubes

Let us now apply these findings to CNTs in an electric field. The bending stiffness of SWCNTs of radius R_{CNT} has been computed using molecular dynamics simulations to approximately follow:[46]

$$a_{\mathrm{CNT}} = 63.80 \, (R_{\mathrm{CNT}} / \text{Å})^{2.93} \, eV \, \text{Å} \qquad (45)$$

Armchair CNTs with chiral vector (n, n) are conductive and have radius:[44]

$$R_{\mathrm{CNT}} \approx \frac{3n}{2\pi} 1.421 \, \text{Å} \qquad (46)$$

We will also assume that the electric field vanishes in the direction of the CNT contour inside a constant cross-section $A_{\mathrm{CNT}} = \pi R_{\mathrm{CNT}}^2$. Taking a temperature of $T = 1200$ K typical for the FCCVD process,[47] we can determine the minimum electric field strength $E_{\min}$ necessary to reach a minimum MCA $\alpha \equiv \langle \hat{\mathbf{t}} \cdot \hat{\mathbf{E}} \rangle_{\min}$ of the chain with the field as a function of CNT length. We choose to find the field strength for a minimum MCA of $\alpha = 0.95$, which corresponds to a minimum average alignment angle of approximately 18°. This value is typical for aligned CNT fibers[48] and lies within the range where our analytical solutions give an accurate prediction of the exact behavior as discussed in Section 4. The exact numerical solutions and the approximations found in Equation (28) are shown in **Figure 5**a for armchair SWCNTs with different chiral vectors. As predicted, we find two regimes separated by a threshold length L^*. Well below L^*, that is, in the rigid rod limit, the electric field strength decreases with a power law. Above L^*, the behavior is dominated by bending effects and the electric field strength converges to a constant value. The exact numerical values for the minimum electric field strength visually coincide with the approximate values computed with Equation (28) apart from one decade around L^* where the system transitions from the short to the long chain limit. Figure 5b shows a generalization of Figure 5a for continuous CNT radii with the exact electric field value. As expected, the electric field strength necessary to reach an certain minimum MCA α reduces with increasing CNT length and radius. We find that for individual SWCNTs, the electric field strength to achieve strong alignment with the field exceeds 10^6 V m^{-1}. This suggests that it is practically impossible to align individual SWCNTs with a static electric field without risking substantial arcing due to electric breakdown of the surrounding gas. However, CNTs form bundles, due to weak van der Waals interactions, which exhibit higher stiffness and have a greater cross-sectional area compared to individual CNTs.[49] Furthermore, multi-walled CNTs (MWCNTs) are also known to be stiffer compared to SWCNTs.[50] The higher stiffness and effective cross-sectional area of these structures may significantly lower the necessary electric field strength for alignment. We remark that the theory as presented here is purely classical in nature and does not take into account any quantum
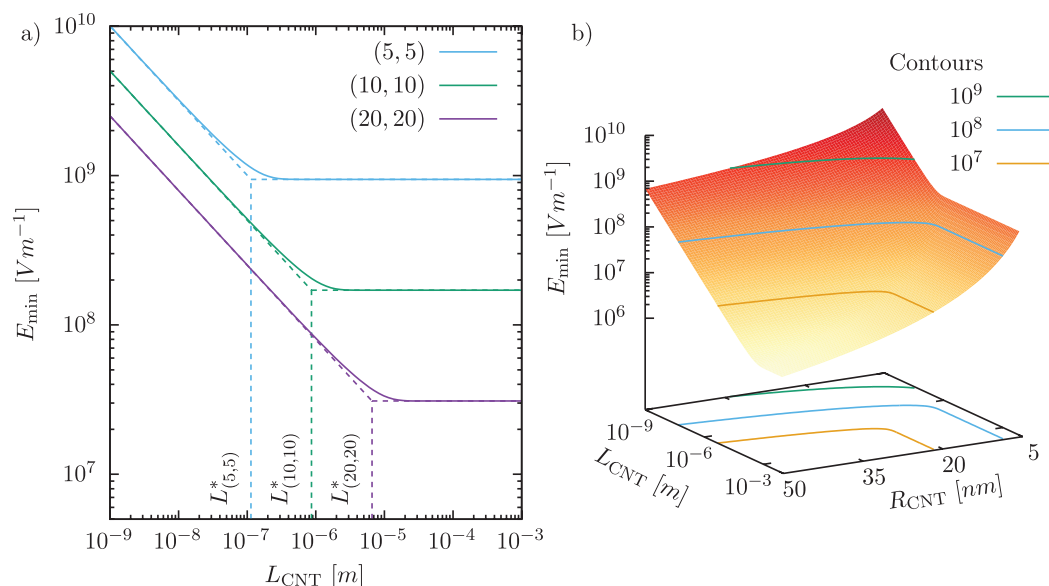
Figure 5. Minimum electric field strength necessary for a minimum MCA value of $\alpha = 0.95$ for SWCNTs. In a), log-log of field strength vs. CNT length for different SWCNTs with chiral vectors listed in the legend. Solid and dashed lines show exact and approximate values respectively. Vertical dashed lines indicate the threshold length L^* for the approximate expression. In b), log-log-lin plot of field strength (log) as a function of CNT length (log) and CNT radius (lin). Isocontours for the field strength are shown on the surface and projected into the xy-plane. A continuous distribution of CNT radii was assumed.

effects that might play a role on the nanoscale, for example, the effect of crystal momentum resonance on conductivity present in CNT junctions.[51] Furthermore, dynamic effects of moving charges may further influence the alignment. An in-depth discussion of these phenomena at this point however would be beyond the scope of this work.

6. Conclusion

Using Ginzburg–Landau theory and the WLC model, we studied the statistics of a freely suspended macromolecule in an aligning field of arbitrary order. By applying a small-angle approximation, simple closed-form solutions for the MCA, an orientational order parameter and the two-point correlation function for the tangent vector along the contour of the chain were derived. In particular, all results in this work can be expressed as compositions of exponential and hypergeometric functions. The results were shown to be in excellent agreement with MC simulations of the exact WLC model in the limit of strong fields and resulting alignment angles of less than 20°. As expected, we found that higher field strengths, greater field coupling and higher bending stiffness lead to greater average alignment of the chain with the external field. An interpolation formula for force–extension curves was derived and compared to results from existing literature. The force–extension curve from the small-angle approximation was found to agree well with the exact solution of the WLC model for strong aligning fields, whereas the interpolation formula gave similar or better agreement with the exact solution than a widely known result due to Marko and Siggia.[8] Approximate expressions and a lower bound for the minimum field strength required to reach a minimum MCA of the chain

contour with the field were computed. All results were found to be consistent with classically derived results for the WLC in the limit of no external field. Furthermore, we confirmed the well-known result that semiflexible chains can be approximately treated as rigid rods if the chain length does not exceed the persistence length. As an example, we derived free energy expressions for an electrically conductive and a linearly dielectric chain in a homogeneous electric field and showed that such a system can be described with our model. As an application of the model, we applied our theory to the alignment of individual SWCNTs with an electric field and showed how the minimum field strength required to reach a desired minimum MCA with the field behaves as a function of the CNTs' parameters.

Acknowledgements

Conflict of Interest

The authors declare no conflict of interest.

Keywords

[1] B. Maier, U. Seifert, J. O. Rädler, *Europhys. Lett. (EPL)* **2002**, *60*, 622.

[2] A. Bensimon, A. Simon, A. Chiffaudel, V. Croquette, F. Heslot, D. Bensimon, *Science* **1994**, *265*, 2096.

[3] R. Lavery, A. Lebrun, J. Allemand, D. Bensimon, X. Croquettev, *J. Phys.: Condens. Matter* **2002**, *14*, R383.

[4] Y. Zhang, A. Chang, J. Cao, Q. Wang, W. Kim, Y. Li, N. Morris, E. Yenilmez, J. Kong, H. Dai, *Appl. Phys. Lett.* **2001**, *79*, 3155.

[5] T. S. Gspann, S. M. Juckes, J. F. Niven, M. B. Johnson, J. A. Elliott, M. A. White, A. H. Windle, *Carbon* **2017**, *114*, 160.

[6] P. Lilienfeld, *J. Aerosol Sci.* **1985**, *16*, 315.

[7] M. Doi, S. Edwards, S. Edwards, *The Theory of Polymer Dynamics*, International series of monographs on physics, Clarendon Press, **1988**.

[8] J. F. Marko, E. D. Siggia, *Macromolecules* **1995**, *28*, 8759.

[9] A. Lamura, T. W. Burkhardt, G. Gompper, *Phys. Rev. E* **2001**, *64*, 061801.

[10] P. Benetatos, E. Frey, *Phys. Rev. E* **2004**, *70*, 051806.

[11] Y. Hori, A. Prasad, J. Kondev, *Phys. Rev. E* **2007**, *75*, 041904.

[12] R. Petrosyan, *Rheol. Acta* **2017**, *56*, 21.

[13] A. Zee, *Quantum Field Theory in a Nutshell* (second ed.), Princeton University Press, **2010**.

[14] T. Vilgis, *Phys. Rep.* **2000**, *336*, 167.

[15] B.-Y. Ha, D. Thirumalai, *J. Chem. Phys.* **1997**, *106*, 4243.

[16] R. G. Winkler, *J. Chem. Phys.* **2003**, *118*, 2919.

[17] A. J. Spakowitz, Z.-G. Wang, *Macromolecules* **2004**, *37*, 5814.

[18] S. Mehraeen, B. Sudhanshu, E. F. Koslover, A. J. Spakowitz, *Phys. Rev. E* **2008**, *77*, 061803.

[19] A. J. Spakowitz, *Europhys. Lett. (EPL)* **2006**, *73*, 684.

[20] J. Samuel, S. Sinha, *Phys. Rev. E* **2002**, *66*, 050801.

[21] S. Stepanow, G. M. Schütz, *Europhys. Lett. (EPL)* **2002**, *60*, 546.

[22] T. Odijk, *Macromolecules* **1983**, *16*, 1340.

[23] T. Odijk, *Macromolecules* **1986**, *19*, 2313.

[24] T. W. Burkhardt, *J. Phys. A: Math. Gen.* **1995**, *28*, L629.

[25] T. W. Burkhardt, *J. Phys. A: Math. Gen.* **1997**, *30*, L167.

[26] J. Z. Y. Chen, *Macromolecules* **2013**, *46*, 9837.

[27] J. Z. Chen, *Prog. Polym. Sci.* **2016**, *54–55*, 3, the Effects of Confinement on Polymeric Thermal Transitions and Nanostructuring.

[28] D. A. Smith, *J. Phys. A: Math. Gen.* **2001**, *34*, 4507.

[29] O. Kratky, G. Porod, *Recl. Trav. Chim. Pays-Bas* **1949**, *68*, 1106.

[30] K. Binder, *Rep. Prog. Phys.* **1997**, *60*, 487.

[31] F. Manca, S. Giordano, P. L. Palla, F. Cleri, L. Colombo, *J. Phys.: Conf. Ser.* **2012**, *383*, 012016.

[32] F. Manca, S. Giordano, P. L. Palla, F. Cleri, L. Colombo, *J. Chem. Phys.* **2012**, *137*, 244907.

[33] J. Blundell, E. Terentjev, *Soft Matter* **2011**, *7*, 3967.

[34] L. Landau, E. Lifshitz, *Statistical Physics* (third ed.), Butterworth-Heinemann, Oxford **1980**.

[35] F. Olver, D. Lozier, R. Boisvert, C. Clark, *NIST Handbook of Mathematical Functions*, Cambridge University Press, **2010**.

[36] R. Roe, W. R. Krigbaum, *J. Chem. Phys.* **1964**, *40*, 2608.

[37] C. R. Desper, R. S. Stein, *J. Appl. Phys.* **1966**, *37*, 3990.

[38] M. Gurp, *Colloid Polym. Sci.* **1995**, *273*, 607.

[39] D. Frenkel, B. Smit, *Understanding Molecular Simulation* (second ed.), Academic Press, San Diego **2002**.

[40] S. Iijima, *Nature* **1991**, *354*, 56.

[41] J. N. Wang, X. G. Luo, T. Wu, Y. Chen, *Nat. Commun.* **2014**, *5*, 1.

[42] Y.-L. Li, I. A. Kinloch, A. H. Windle, *Science (New York, N.Y.)* **2004**, *304*, 276.

[43] C. Martin, J. Sandler, A. Windle, M.-K. Schwarz, W. Bauhofer, K. Schulte, M. Shaffer, *Polymer* **2005**, *46*, 877.

[44] R. Saito, G. Dresselhaus, M. Dresselhaus, *Physical Properties Of Carbon Nanotubes*, World Scientific Publishing Company, Singapore **1998**.

[45] A. Kaniyoor, J. Bulmer, T. Gspann, J. Mizen, J. Ryley, P. Kiley, J. Terrones, C. Miranda-Reyes, G. Divitini, M. Sparkes, B. O'Neill, A. Windle, J. A. Elliott, *Nanoscale* **2019**, *11*, 18483.

[46] L. V. Zhigilei, C. Wei, D. Srivastava, *Phys. Rev. B* **2005**, *71*, 165417.

[47] L. Weller, F. R. Smail, J. A. Elliott, A. H. Windle, A. M. Boies, S. Hochgreb, *Carbon* **2019**, *146*, 789.

[48] N. Behabtu, C. C. Young, D. E. Tsentalovich, O. Kleinerman, X. Wang, A. W. K. Ma, E. A. Bengio, R. F. ter Waarbeek, J. J. de Jong, R. E. Hoogerwerf, S. B. Fairchild, J. B. Ferguson, B. Maruyama, J. Kono, Y. Talmon, Y. Cohen, M. J. Otto, M. Pasquali, *Science* **2013**, *339*, 182.

[49] A. M. Boies, C. Hoecker, A. Bhalerao, N. Kateris, J. de La Verpilliere, B. Graves, F. Smail, *Small* **2019**, *15*, 1900520.

[50] C. Q. Ru, *Phys. Rev. B* **2000**, *62*, 9973.

[51] R. A. Bell, M. C. Payne, A. A. Mostofi, *Phys. Rev. B* **2014**, *89*, 245426.